Article Contr. Atmos. Phys., November 1999, p. 287–301
0005-8173/99/04 0287-15 $ 3.00/0 Vol. 72, No. 4 287

Simulation of Breaking Gravity Waves during the South Foehn of January 7–13, 1996

HEIDI SCHMID AND ANDREAS DÖRNBRACK

DLR Oberpfaffenhofen, Institut für Physik der Atmosphäre, D-82230 Weßling, Germany

(Manuscript received July 9, 1998; accepted December 17, 1998)

Abstract

A high-resolution mesoscale model with horizontal mesh size of 6 km is applied to simulate upper-level wave breaking above the Alps during a south foehn event in January 1996. The model reproduces the key synoptic and mesoscale features of cross-alpine airflow during foehn. High-vertical resolution radiosonde soundings at Munich and Innsbruck are used to evaluate the quality of the model simulations. The simulations predict breaking gravity waves above the jet stream in a layer between 10 and 15 km altitude where the shear is maximum. In part of the foehn period a critical level is present at about 200 hPa that results in wave steepening below and no wave activity aloft. Regions where aircraft report clear-air turbulence encounters agree reasonably with the simulated locations of gravity wave breaking.

1 Introduction

Clear-air turbulence (CAT) is known to occur in regions of large vertical shear associated with distinctive synoptic-scale features such as jet stream and frontal zones (Keller, 1990; Knox, 1997). In this setting scale-contraction of the synoptic flow results in a vertical structure characterized by low values of the Richardson number and the occurrence of CAT in the form of Kelvin-Helmholtz instability (Dutton and Panofsky, 1970). Furthermore, significant topographic features such as the Rocky Mountains and the Alps modify the incident flow and can induce upward propagating gravity waves that, if of sufficient amplitude, can overturn and break to yield CAT (e.g. Lilly, 1978). The wave breaking can occur at elevations varying from the mid-troposphere to the mid-stratosphere.

Observations of CAT are hampered by its 'clear-air' nature and sporadic occurrence at locations and elevations that makes monitoring difficult. These properties have hindered the compilation of an adequate CAT climatology, and the acquisition of detailed measurements of its evolution and structure.

It has long been recognized that the avoidance of CAT encounters by aircraft can benefit airlines in terms of passenger safety and comfort as well as economic performance. However, unexpected CAT encounters are still one of the primary risks for aeronautics. Recent technological progress in remote sensing techniques and the use of high-performance computers may help to extend our knowledge of the synoptic- and mesoscale processes leading to CAT. Additionally, CAT forecasts by air safety agencies and weather aviation services can become more trustworthy by using results of these new technologies.

The development of Doppler lidar systems enabled the observation of temporally and spatially high-resolved fields of wind and backscatter intensity (e.g. Ralph et al., 1997). Furthermore, airborne lidar methods are currently developed that allow the detection of CAT regions up to 20 km ahead of the aircraft.

Although a reliable CAT forecast by existing operational numerical models (minimum horizontal resolution of $\Delta x \approx 20$ km) is not yet possible, research-type high-resolution models ($\Delta x \approx 1$ km) resolve at least the background flow conditions where CAT can be locally produced. Simulations resolving the turbulence directly ($\Delta x \leq 100$ m) need special numerical tools as large-eddy simulation codes; currently, these methods are mostly restricted to idealized flow structures (e.g. Dörnbrack, 1998).

In the last decades our understanding of airflow around and over topography has been improved significantly (e.g. Smith, 1979; Baines, 1995; Wurtele et

al., 1996). However, relatively little is known about the three-dimensional nature of wave generation, propagation and the wave breaking over complex topography. Therefore, simulation of breaking gravity waves at upper flight levels represents an outstanding opportunity to demonstrate that numerical mesoscale models can accurately predict aircraft data reported CAT regions. Here, we investigate upper-level wave breaking and mountain-wave induced CAT above the Alps by mesoscale numerical simulation. The emphasis of this study is the comparison of model results with radiosonde data and aircraft data reports.

The orientation of the main ridge of the Alps is roughly east-west. Southerly flow past the Alps may generate the so-called south foehn occuring north of the mountain range whereas north foehn is blowing south of the mountains in northern Italy. North as well as south foehn events are expected to generate substantial upper-level gravity wave activity (for a statistics of Alpine foehn events, see Hoinka, 1990). Because busy air traffic routes[1] are located over the Alps, this area is susceptible to mountain wave and turbulence encounters.

A research-type mesoscale model is applied to simulate the cross-alpine flow and the vertical propagation and overturning of gravity waves during a south foehn event in January 1996 using a minimum horizontal resolution of $\Delta x = 6$ km. On a recent meeting of the Mesoscale Alpine Programme (MAP, Binder and Schär, 1996) modelling group it has been suggested to intercompare the gravity wave breaking by different mesoscale models. The MAP data centre (`http://www.map.ethz.ch`) contains meteorological data and simulation results of selected foehn cases where clear-air turbulence was reported by pilots. In this frame, our paper can be understood as a contribution to the high-resolution model intercomparison in the pre-field phase of MAP.

The outline of the paper is as follows. Section 2 describes the mesoscale model set-up and results are presented in Section 3. The model results are compared with observations (radiosonde data, aircraft data reports) in Section 4. Finally, conclusions are drawn in Section 5.

2 Mesoscale Model Set-up

In this study we investigate mesoscale meteorological conditions where mountain-induced gravity waves lead to a local generation of clear-air turbulence in the upper troposphere/lower stratosphere (free atmosphere) during the foehn event from 7 till 13 January 1996.

The fifth generation Pennsylvania State University / National Center for Atmospheric Research mesoscale model (MM5, Grell et al., 1994) is used to study the tropospheric and stratospheric wave structure. The model integrates the fully compressible set of equations in a rotating frame of reference. In the nonhydrostatic version used here velocity, pressure perturbation and temperature are the prognostic variables; turbulent kinetic energy is not explicitly calculated in this version of MM5.

The model domain is centred around the Alps with an extension of 3294 km × 3294 km. Thus, a distance of about 1000 km is left between the lateral boundaries and the Alpine mountain range. This diminishes the interaction between the orographically induced airflow and the domain boundaries. Furthermore, the central position of the Alps as the main source of mountain waves facilitates simulations with a twofold local grid refinement (nested domains) to resolve most of the spectrum of orographically induced waves in the free atmosphere. The horizontal mesh size of the outer domain is $\Delta x =$ 54 km, the grid lengths of the two nested domains amount to 18 and 6 km, respectively. The innermost domain extends over 726 km × 726 km and covers almost the entire Alps (see Figure 1). Terrain heights on the finest grid were obtained by interpolation from a 30″ orographic data set provided by the Geophysical Data Center (Boulder). According to estimates of Leutbecher (1998), the shortest horizontal wavelength resolved by the numerical model is about $10\Delta x$, i.e. about 60 km.

The model uses scaled reference pressure as vertical coordinate. The equidistant vertical resolution Δz amounts to approximately 470 m in every domain. In total 45 levels are used up to the model top at 50 hPa ($\approx$ 20 km). There, a radiative boundary condition avoids the reflection of vertically propagating gravity waves.

Radiative and moist processes are switched off as the prime concern lies on the dynamics of mountain wave-induced turbulence at upper levels. The boundary layer is parameterized by a standard bulk formulation ($\tau \propto -\rho u^2$) whereas turbulent mixing in the free atmosphere is taken into account by vertical diffusion which depends on the local Richardson number Ri according to

$$K_v = \begin{cases} K_0 + l_K^2 S \dfrac{Ri_c - Ri}{Ri_c} & , \quad \text{for } Ri < Ri_c \\ K_0 & , \quad \text{for } Ri \geq Ri_c, \end{cases}$$

[1] About 3000 aircraft cross the Alps daily.

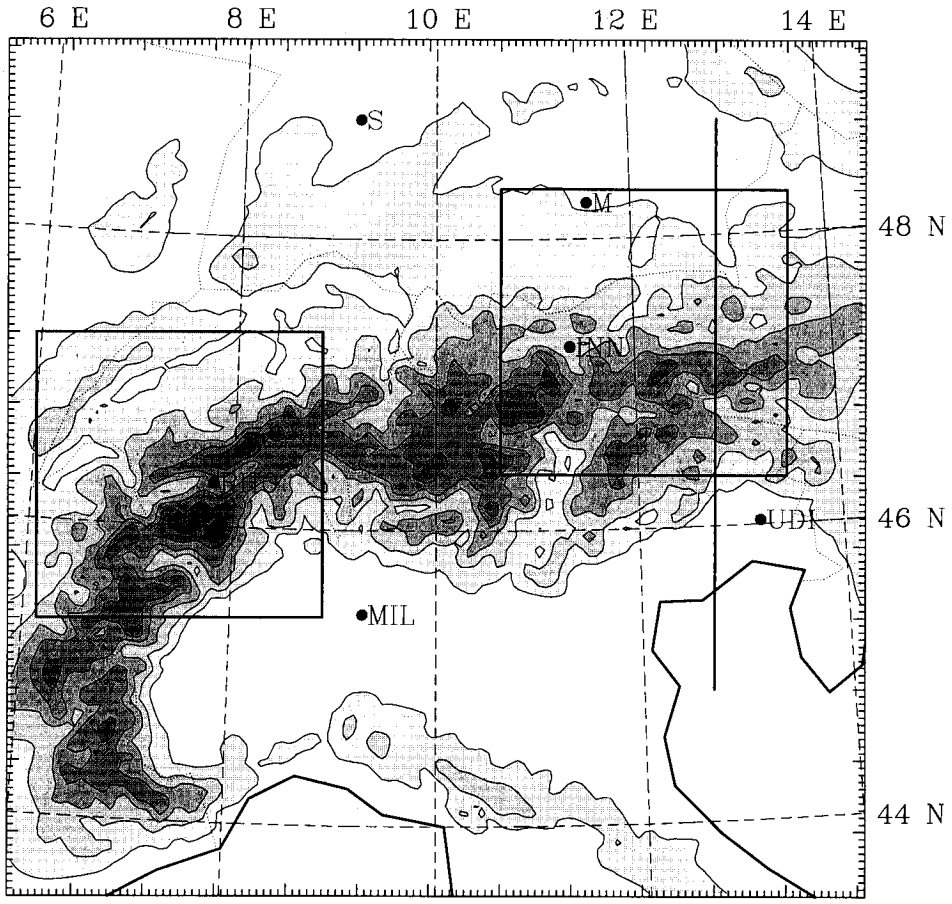

Figure 1: Model orography of the Alps given in increments of 500 m inside the second nested computational domain. Locations: Munich (M), Stuttgart (S), Innsbruck (INN), Rhône valley (RHO), Milan (MIL) and Udine (UDI). Indicated are the cross-section through the eastern Alps (Tauern region) and two subdomains shown in Figures 6 and 13. The tics mark the horizontal grid points with a spacing of 6 km.

where $l_K = 40$ m. The Richardson number Ri is defined as

$$Ri = \frac{N^2}{S^2}$$

where

$$N = \sqrt{\frac{g}{\vartheta}\frac{\partial \vartheta}{\partial z}}$$

and

$$S = \left[\left(\frac{\partial u}{\partial z}\right)^2 + \left(\frac{\partial v}{\partial z}\right)^2\right]^{1/2}$$

are the buoyancy frequency N and the magnitude of the vertical shear S. The critical Richardson number $Ri_c = 0.257(\Delta z)^{0.175}$ and the uniform part of the vertical diffusion $K_0 = 0.001\Delta z$ m s^{-1} depend on the local vertical mesh size Δz.

Two simulations of 48 h and 60 h cover the period from 9 January 00:00 UTC till 13 January 1996, 00:00 UTC. The initial conditions and boundary values were prescribed by 12 hourly analyses of the European Centre for Medium-Range Weather Forecasts (ECMWF) with a horizontal resolution of 2.5° in latitude and longitude and 13 levels between the surface and the 50 hPa pressure level.

3 Model Results

3.1 Synoptic Overview

The long-lasting south foehn event from 7 till 13 January 1996 was caused by a large and stable pressure gradient over Europe. A nearly stationary high pressure system was situated over eastern Europe whereas three intense surface depressions (minimum central pressure: 945 hPa on 9 January) were moving successively from the North-Atlantic ocean towards

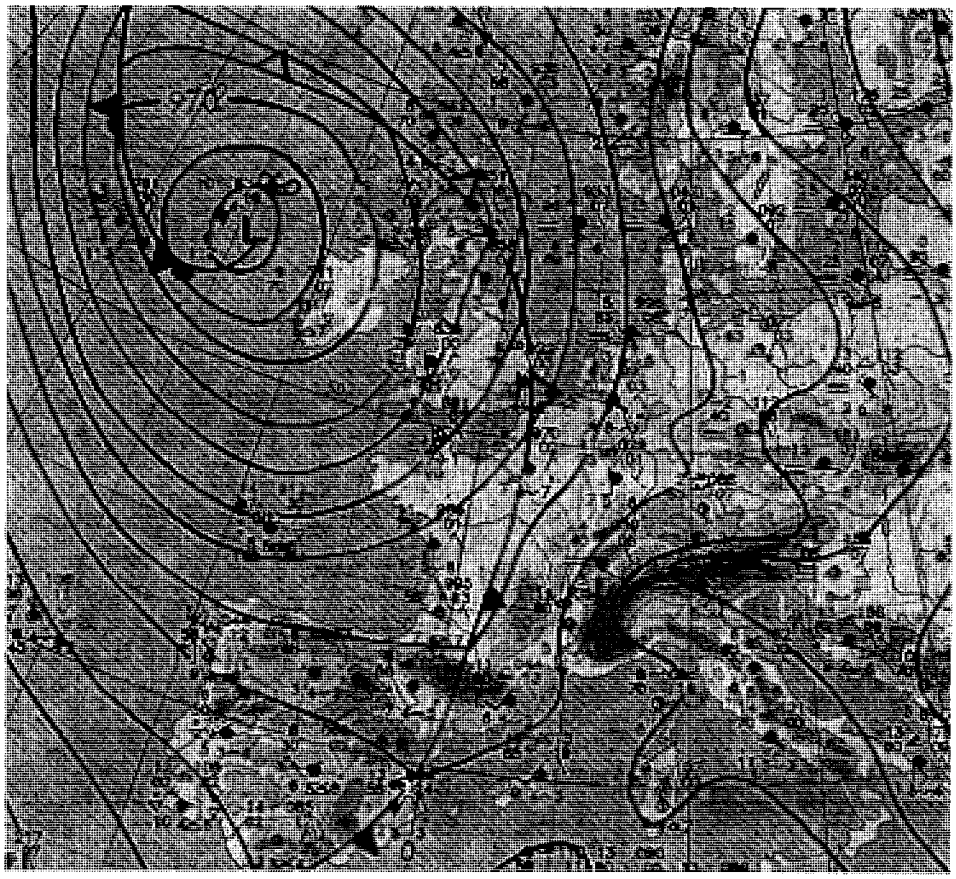

Figure 2: Surface weather chart on 12 January 1996 00:00 UTC containing station reports and pressure analysis (increment 5 hPa; adapted from Europäischer Wetterbericht).

the north-west coast of Ireland. This synoptic surface pressure distribution resulted in persistent southerly winds across the Alps.

As a typical example of the synoptic situation, Figure 2 represents the surface weather chart of 12 January 00:00 UTC where one of the depressions is located west of Ireland. Above the Alpine mountain range, the foehn-like mesoscale pressure distribution, i.e. a lee-trough north of the Alps and high pressure (the so-called foehn nose) over northern Italy, caused strong and gusty low-level winds on the entire lee slope.

Another kind of synopsis is given by the infrared satellite image of 11 January 1996, 12:18 UTC (Figure 3). In the west, the bright N–S orientated cloud band indicates the cold front of the North-Atlantic low. Over Italy, southerly winds transport moist air towards the Alps. The blocking produces low-level clouds covering the up-wind side which can be seen as uniform grey regions over northern Italy. Downstream of the main ridge the descending air dries and the view is opened on the snow-covered Alpine foreland. There, cloud bands (*altocumulus lenticularis*) with a range of orientations about NW–SE can be seen. These clouds are taken to be the visible manifestation of tropospheric lee waves with horizontal spacing of about 20 km. The cloud gap (also called foehn window, see Hoinka, 1990) is bounded by a sharp cloud edge on its north-eastern side.

Optimum upstream conditions for the excitation and vertical propagation of gravity waves can be deduced by means of linear wave theory (e.g. Smith, 1977; Shutts, 1995). The wind speed at crest level must be high and the wind direction nearly perpendicular to the mountain ridge for a significant excitation of gravity waves. The Froude number $\mathcal{F} = U/Nh_0$ characterizes the flow regime, where U and N are the mean upstream wind speed and the buoyancy frequency of the low-level flow, respectively. Essentially, for $\mathcal{F} > 1$ the oncoming flow has enough kinetic energy to pass over the crest height h_0 of the mountain. For $\mathcal{F} < 1$, the flow is partially or totally blocked and becomes diverted around the mountains (Pierrehumbert and Wyman, 1985; Baines, 1995). Moreover, the turning of the wind vector with height must be small in order to avoid absorption of upward propagating gravity waves at critical layers where the phase speed of the wave equals the mean flow speed (Booker and Bretherton, 1967).

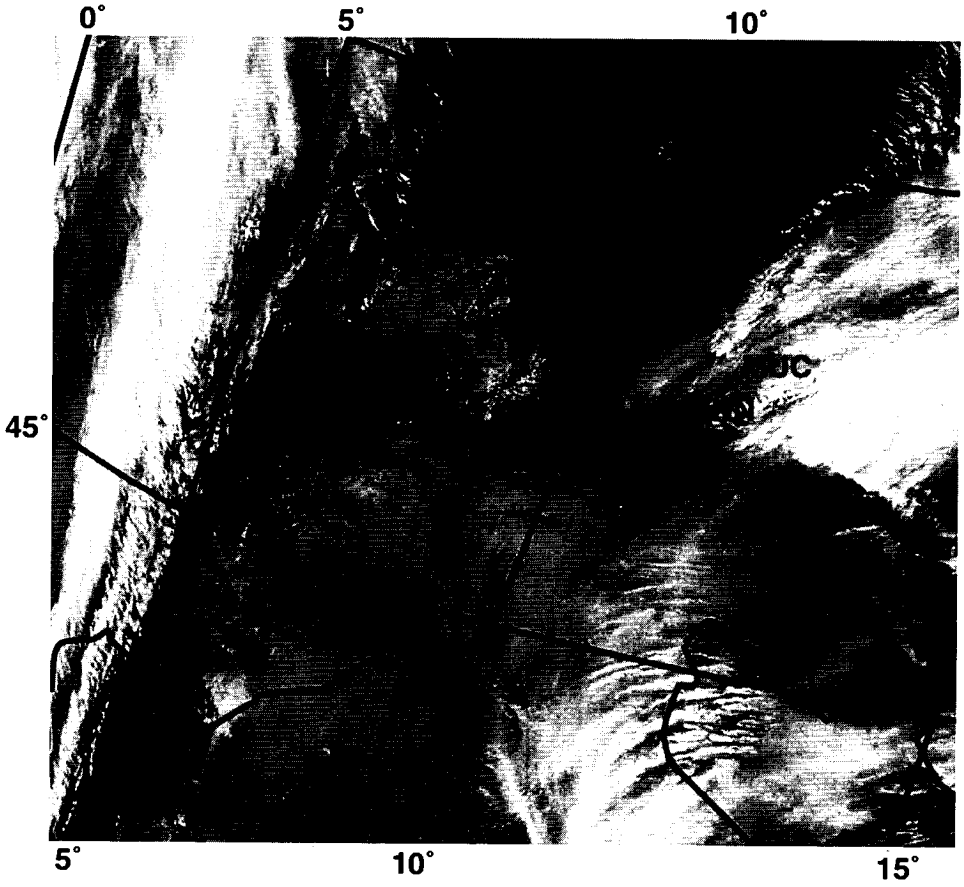

Figure 3: High resolution infrared NOAA-14 satellite image (channel 4) on 11 January 1996 12:18 UTC (adapted from the regular World Wide Web information provided by University of Dundee, UK).

During the foehn period, the horizontal wind vector V_H is nearly perpendicular to the main ridge of the Alps and its meridional component will be denoted by $U_\perp$. The temporal evolution of the upstream velocity $U_\perp$ at different levels is derived from radiosonde soundings at Milan (Figure 4a). A marked increase of the horizontal wind speed at all levels occurs on 8 January afternoon. Afterwards, $U_\perp$ stays nearly constant until 11 January. Low-level winds at 700 hPa are on average 10 m s^{-1} with maximum values up to 15 m s^{-1}. In the lower stratosphere, the wind direction turns from south to west, north-west above about 200 hPa ($\approx$ 12 km) in the course of 11 January. This indicates the presence of a critical level for vertically propagating mountain waves. Observations of the Udine soundings as a station upstream of the eastern Alps depict a similar evolution, however, about 8... 10 hours later.

During the persistent period of high tropospheric winds, the directional shear between the 700 hPa level and upper levels (400 and 250 hPa, i.e. about 7 and 10 km) is less than 45° (Figure 4b). The strong low-level winds upstream as well as the weak directional shear facilitate the excitation and optimal vertical propagation of gravity waves up to about 12 km altitude. Higher up wave absorption by critical level is to be expected. Based on these findings, gravity wave activity is expected in the western Alps from 9 January 06:00 UTC till 11 January 12:00 UTC whilst in the eastern Alps the wave activity should be predominant from 10 January 00:00 UTC until the end of the foehn period considered here.

The airflow is partially blocked in front of the Alps, i.e. the air flow stagnates or reverses in the boundary layer (see the 925 hPa level in Figure 4a). In Figure 4c, a local Froude number $\mathcal{F}_p = U_\perp(p)/N(p)$ $(h_0 - z(p))$ is plotted for different pressure levels. The average crest height of the Alps is taken to be $h_0 = 3500$ m and $N(p)$ is the background buoyancy frequency. Although the low-level Froude numbers $\mathcal{F}_p$ increase during the foehn event, they remain significantly below 1. The 700 hPa Froude number reaches values up to 1.8.

As a first estimate, the height of the dividing streamline H_S which separates blocked air from air masses passing the Alps can be calculated by $H_S = h_0[1 -$

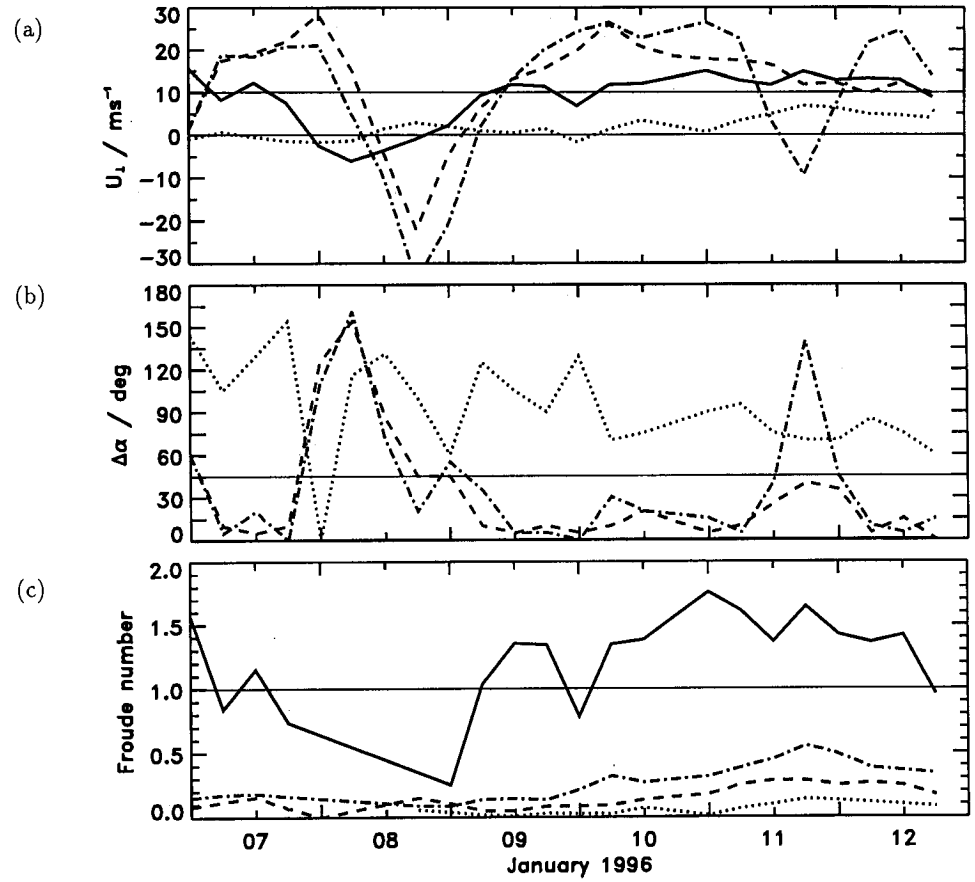

Figure 4: Upstream conditions for Milan during the foehn period. (a): Horizontal wind speed $U_\perp$ (positive values from south to north) perpendicular to the main mountain ridge at heights of 925 hPa (·····), 700 hPa (———), 400 hPa (- - - -) and 250 hPa (- · — · — ·—). (b): Directional shear of the horizontal wind related to the wind direction at 700 hPa, line coding as in (a). (c): Froude numbers $\mathcal{F}_p = U_\perp(p)/N(p)h_p$, where $h_p = 3500\ \text{m} - z(p)$ at 925 hPa (·····), 850 hPa (- - - - -), 800 hPa (- · — · — ·—) and 700 hPa (———). Data are taken from 6 hourly radiosonde ascents.

$U_\perp/(h_0 N)$] (Sheppard, 1956; Snyder et al., 1985). Using $U_\perp \approx 10\ \text{m s}^{-1}$ and $N \approx 0.012\ \text{s}^{-1}$ as mean values of the Milan soundings yields $H_S \approx 2700$ m. This is somewhat lower than the height of the 700 hPa-level (≈ 2.9 km) where $\mathcal{F}_p > 1$. Effectively, an air layer of about 800 m thickness passes over the Alps and causes the orographic forcing of vertical motions.

3.2 Regions of Turbulence and Wave Events

Radiosondes are launched routinely at best every 6 hours. However, the temporal variability of the flow over mountains is much higher as documented by the simulated evolution of hourly wind profiles taken at three model locations MIL, INN and RHO (see Figure 5).

The upstream winds (represented by Milan, Figure 5a) confirm the measurements shown in Figure 4a: tropospheric winds are southerly, the wind speed at crest height (i.e. approximately 3500 m) exeeds 10 m s^{-1} and increases with height up to values of more than 30 m s^{-1} at 10 km during 10 and 11 January. The tropospheric jet weakens during January 11th. In the same period, the stratospheric wind speed decreases and the wind almost reverses direction from the troposphere to the stratosphere indicating a critical level for all stationary mountain waves. At the end of the foehn event, a weak tropospheric jet reappears. However, the low-level wind ceases.

In contrast to the upstream conditions, profiles taken at Innsbruck (Figure 5b) indicate a wave-induced layer of strong vertical shear (≈ -20 m s^{-1} per 1000 m) at an elevation of about 12 km, the upper edge of the jet stream. In the low velocity region above, the wind turns drastically by more than 45°

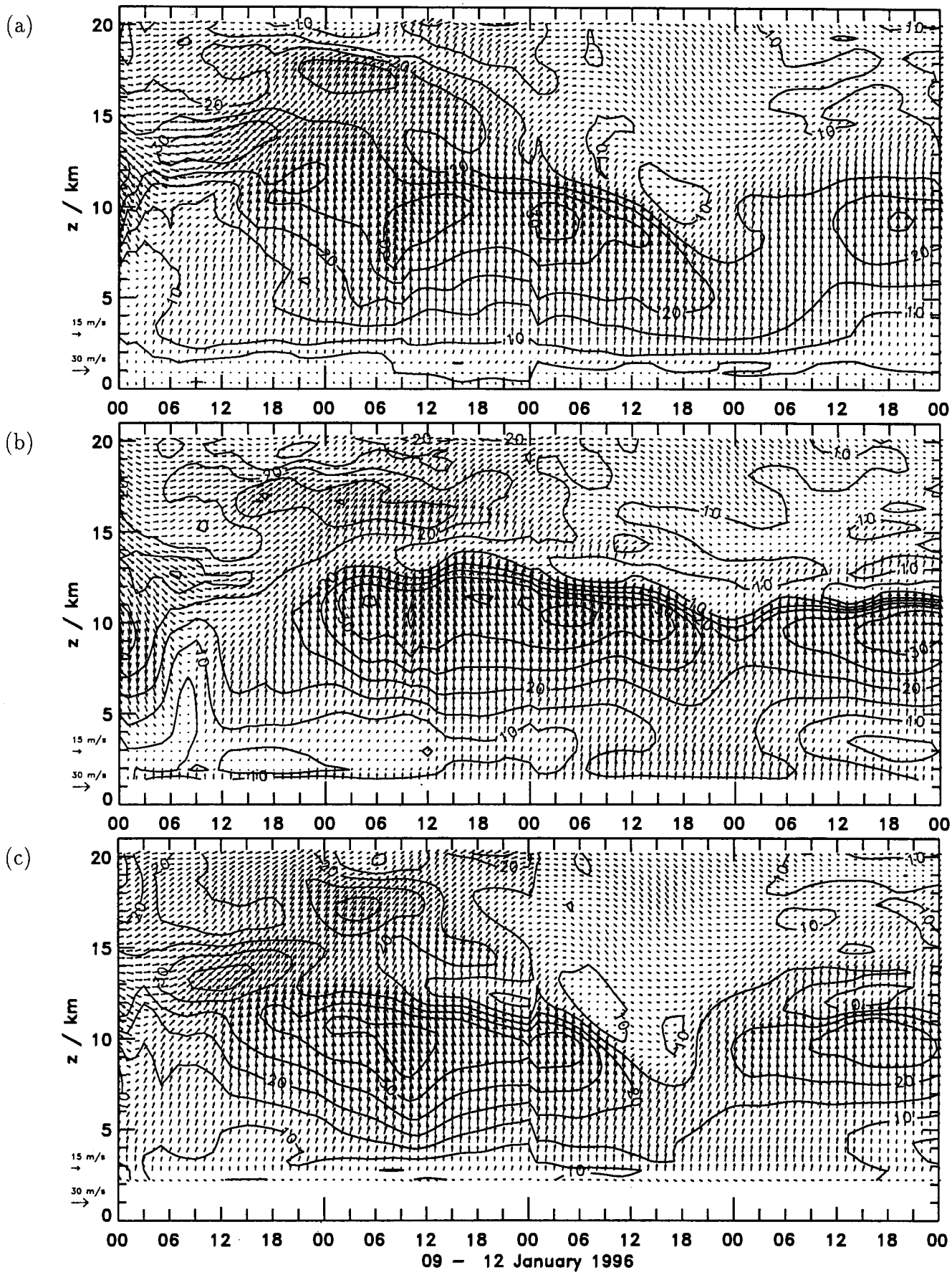

Figure 5: Model profiles of the horizontal wind vector and contours of its magnitude (increment 5 m s^{-1}) at Milan (a), Innsbruck (b) and the location RHO (see Figure 1) in the Rhône valley (c) during the whole simulation period. A slight discontinuity arises at 11 January 00:00 UTC from using data of the later (earlier) simulation after (before) this date.

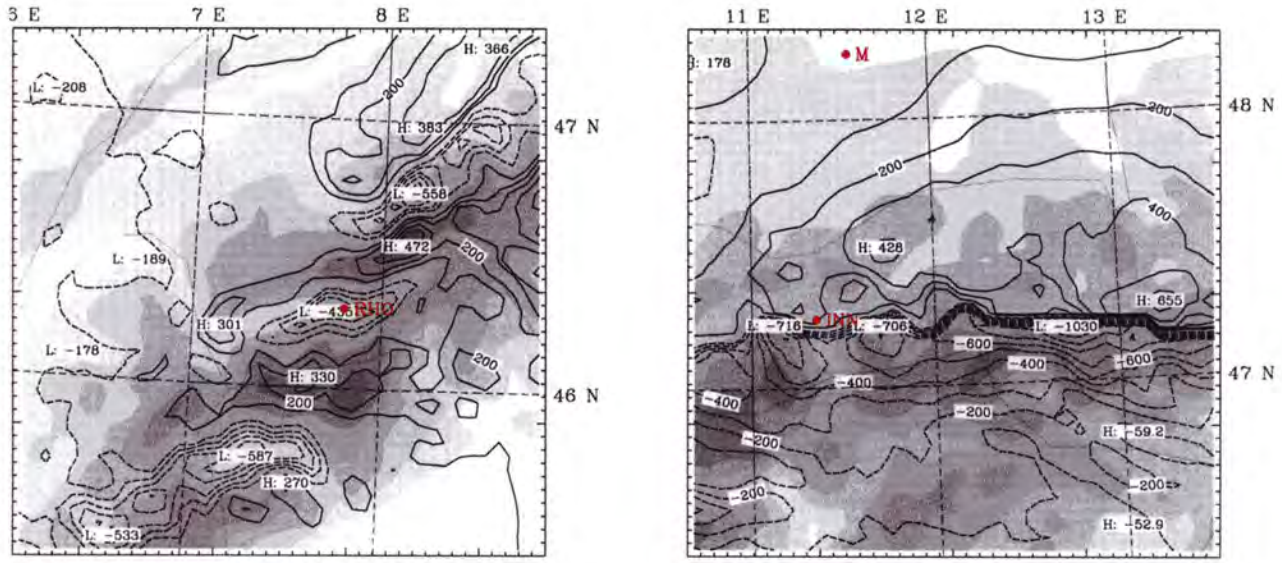

Figure 6a: Wave induced vertical displacement (m) of the disturbances of the 340 K isentropic surface for the western Alps (left, mean height 11.6 km) and of the 380 K isentropic surface for the eastern Alps (right, mean height 14.2 km) on 10 January 1996 18:00 UTC. The model orography is shaded as in Figure 1.

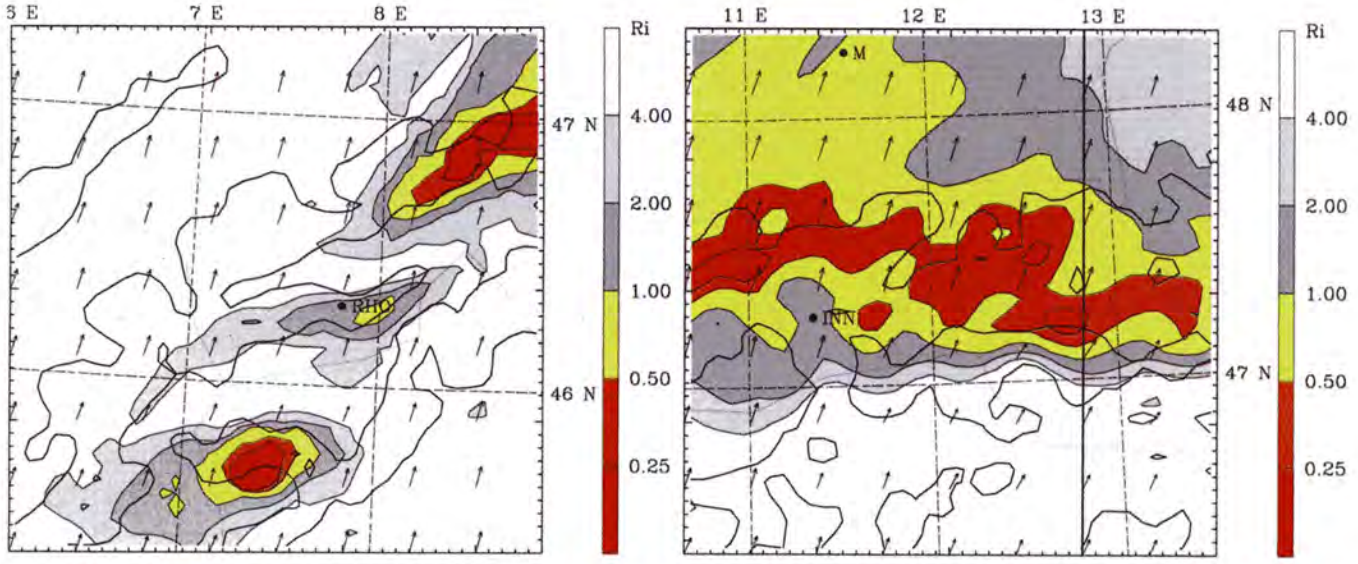

Figure 6b: Minimum Richardson numbers in a column between 8 and 12 km on 10 January 1996 18:00 UTC. The left (right) panel shows the western (eastern) Alps.

from S to SW. Related to the background profiles of Milan or Udine, the deviation in speed and direction is significant and may be a result of a region of breaking gravity waves. This vertical structure starting on 10 January is typical for all stations of the eastern Alps and persists over nearly three days.

At another location inside the mountain range (location RHO, Western Alps, see Figure 1), the comparison with the upstream profiles indicates orographically induced wind speed perturbations only during the first two days of simulation (Figure 5c).

The deviation of the isentropic levels from their respective average height is a measure of the mountain wave amplitude. This is shown above two representative regions of the Alps in Figure 6a. Over the western Alps, the displacements of isentropic surfaces are highly correlated with individual orographic ridges underneath and peak-to-peak amplitudes of up to 1000 m are simulated. In the eastern Alps, the chain of "Zillertaler Alpen" and "Hohe Tauern" acts as one coherent orographic obstacle for the southerly airflow. The breaking of gravity waves can be recognized as extended sharp boundary be-

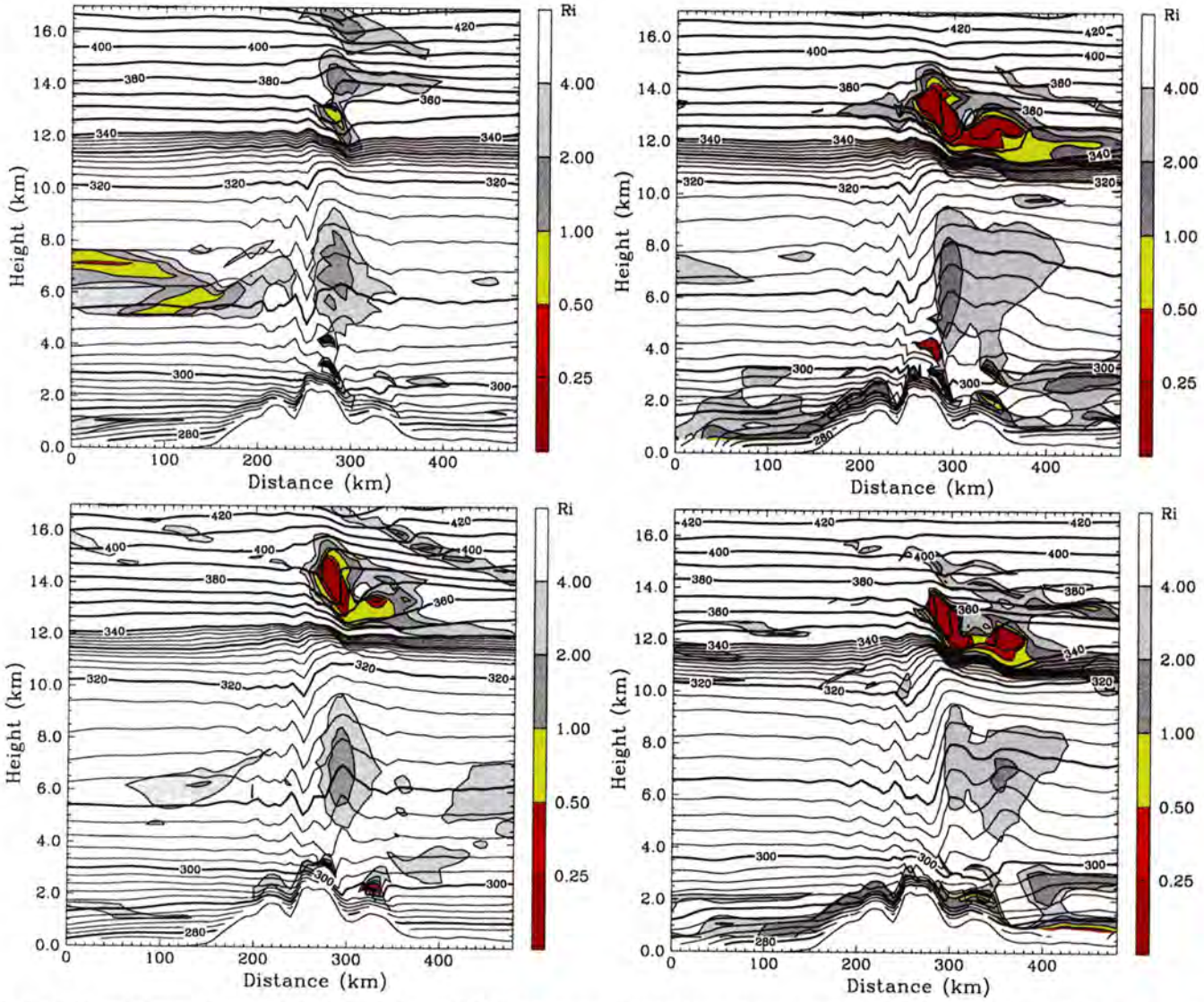

Figure 7: Isentropes (heavy; increment: 5 K) and Richardson number (coloured) in a south-north section through the Tauern region (see Figure 1) on 10 January 1996 12:00 UTC, 18:00 UTC, 11 January 1996 00:00 UTC and 12:00 UTC (from top to bottom and left to right). The terrain height is indicated at the bottom.

tween positive and negative perturbations of isentropic surfaces (Figure 6a). This pattern and the maximum peak-to-peak amplitude of 1700 m point to an overturning gravity wave.

The spatial distribution of the minimum Richardson numbers estimated in a column from 8 to 12 km above both regions characterizes likely source regions of turbulence (Figure 6b). Turbulence production can be expected at a Richardson number of less than about 0.25. Over the western Alps, minimum Richardson numbers are found predominantly on the lee side of individual massifs and summits like "Grajische Alpen" with Gran Paradiso ($\approx$ 45.5°N, 7.5°E), "Waliser Alpen" with Matterhorn ($\approx$ 46.0°N, 7...8°E), and "Berner Alpen" with Jungfraujoch ($\approx$ 45.5°N, 8.1°E). In the eastern Alps, the statically unstable region of the overturning wave causes negative Richardson numbers. An extended area of small Richardson numbers ($Ri < 1$) downstream of the massif and patches of $Ri < 0$ in the lee of the highest peaks (Groß-Venediger, Groß-Glockner) indicate favourable conditions for the local production of turbulence.

The temporal development of the gravity wave breaking is represented by vertical cross sections through the Tauern region (Figure 7). On 10 January 12:00 UTC two spots of reduced Richardson number $Ri < 2$ are found in the troposphere between 5 and 8 km and above the tropopause at 12...15 km. The low Richardson number region on the windward side is mainly caused by strong vertical shear at the lower edge of the tropospheric jet stream whereas

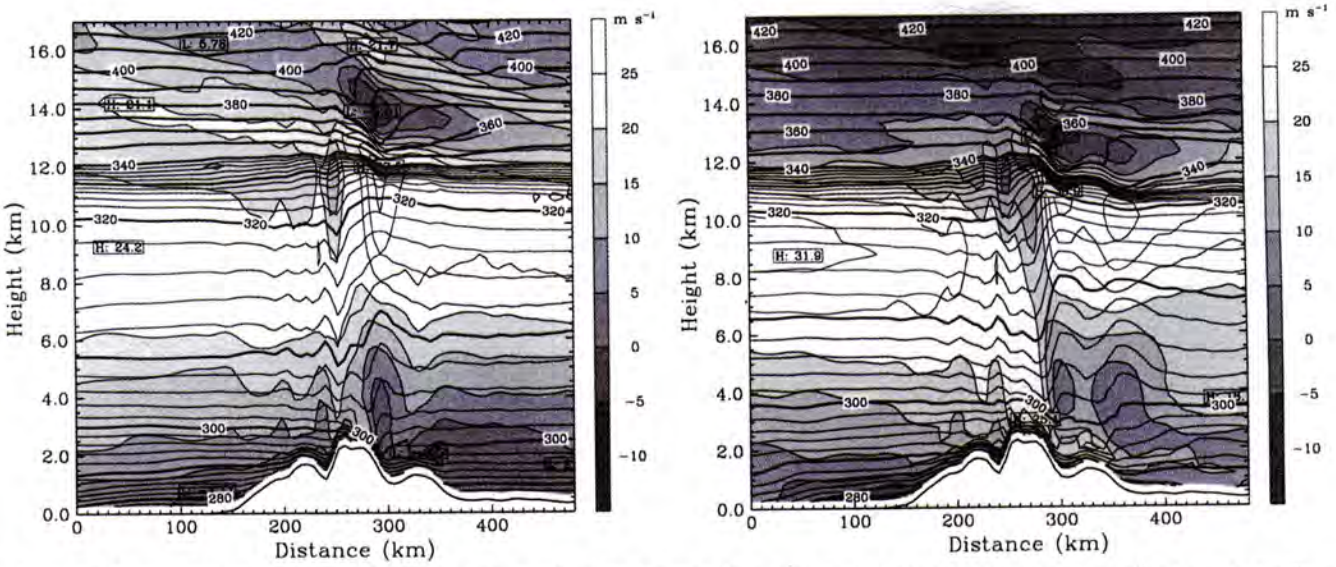

Figure 8: Horizontal wind tangential to the north-south cross section (thin lines and shaded; increment: 5 m s^{-1}) through the Tauern region (see Figure 1) and potential temperature (heavy; increment: 5 K) on 10 January 1996 18:00 UTC (left), and 11 January 1996 12:00 UTC (right).

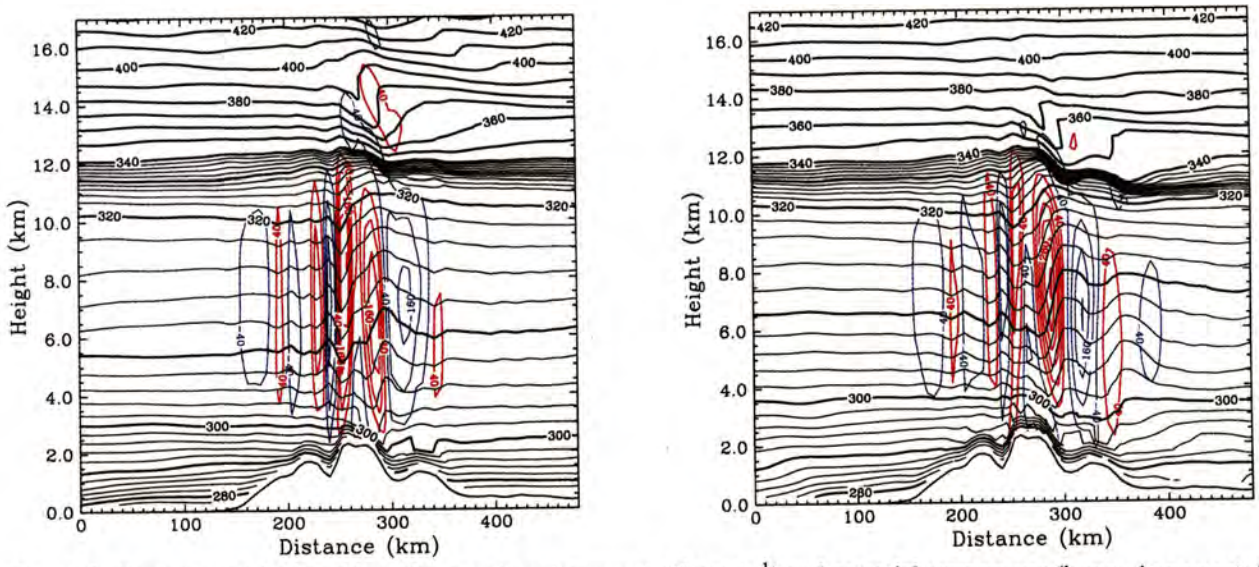

Figure 9: Vertical wind (red positive, blue negative; increment: 40 cm s^{-1}) and potential temperature (heavy; increment: 5 K) in the same cross section and at the same times as indicated in Figure 8.

low Richardson numbers above the Alps are certainly caused by the wave-induced reduction of static stability and the increased shear. Six hours later, the isentropic surfaces between 13 and 15 km overturn above the mountain peaks. Therefore, negative Richardson numbers occur. In these regions, clear-air turbulence is to be expected. The vertical thickness of the breaking region amounts to about 2 km and regions of $Ri < 2$ extend approximately 100 km downstream. The subsequent development (until 11 January 12:00 UTC) is characterized by the stationary position of the wave breaking regions above the Alps, a reduction of wave amplitude and a descent of statically unstable region down to 12 km (Figure 7). On the following days the wave activity weakens and disappears on 13 January 1996.

The horizontal wind tangential to the North-south section through the "Tauern" shown in Figure 8 is nearly perpendicular to the mountain ridge. The most remarkable feature is the tropospheric jet. Its speed has been increased in the preceding days. It is the strong vertical shear at its upper and lower edge which produced the horizontally extendend regions of small Richardson number shown in Figure 7. Furthermore, the horizontal speed is markedly reduced

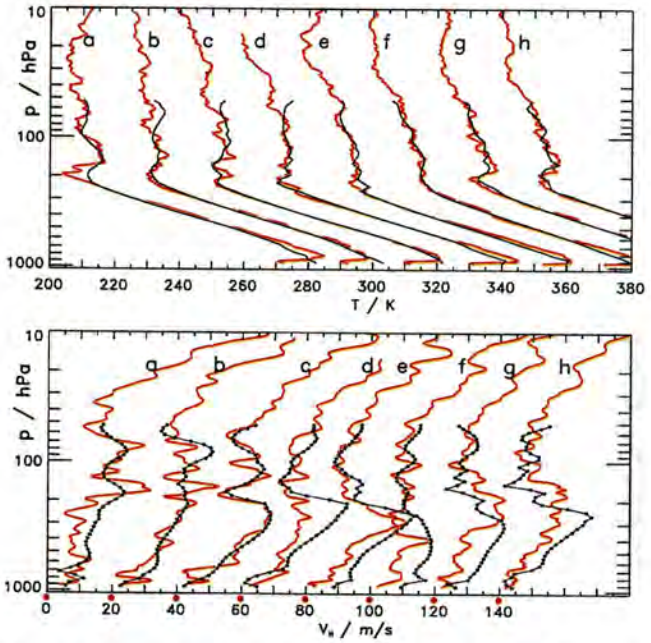

Figure 10: Fine resolution radiosondes and model profiles of temperature (top), horizontal wind speed ((bottom) for Munich (see Figure 1) from 9 January 12:00 UTC (a) til 13 January 00:00 UTC (h) every 12 hours. The measurements (every 10 s $\approx$ 50 m vertical resolution) are marked by red lines, the model profiles by black lines with dots indicating the model levels. Profiles (b) to (h) are shifted by 20 K (20 m s^{-1}). The origin of each velocity profile is marked by an enlarged dot on the abscissa.

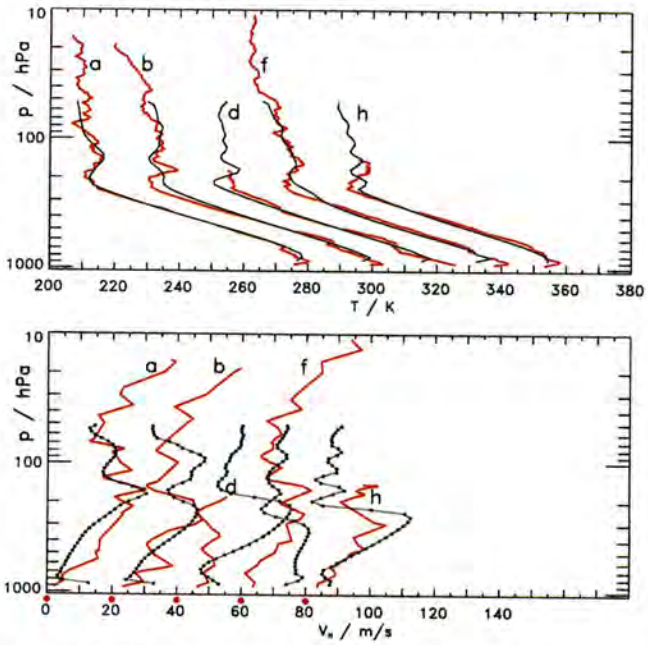

Figure 11: Radiosondes and model profiles of temperature (top), horizontal wind speed ((bottom) for Innsbruck (see Figure 1) from 00:00 UTC on 9 January (a) till 13 January 00:00 UTC (h) every 24 hours. Details are as in Figure 10 apart from the resolution of the measured wind profile. This was available on standard pressure and significant levels only.

to even negative values in the wave breaking region as expected for overturning waves. Below the jet stream the horizontal velocity decreases down to the surface. On the upstream side, stagnant and reversing flow prevails for $z < 2$ km whereas a clear increase of the wind velocity by foehn is recognizable on the lee side on 11 January 12:00 UTC. At this time, the maximum speed at crest level is nearly 25 m s^{-1} and the vertical velocity above the mountain ridges achieves values of 2.5 m s^{-1} in the mid-troposphere (Figure 9). Above the tropopause, the vertical wind is much smaller (maximum 0.5 m s^{-1}). The upstream tilt of wave phase is evident only in the stratosphere.

4 Comparisons with Observations

4.1 Radiosonde Soundings

High-vertical resolution radiosonde soundings of wind and temperature are valuable data for evaluating mesoscale model results. They have a vertical resolution of about 50 m, i.e. approximately 500 vertical levels contribute to the profiles up to the burst height of the balloon. The accuracy of the Väisälä temperature sensors is ± 0.1 K whereas the velocity is accurate within ± 1 m s^{-1}.

Figure 10 presents the temperature and wind soundings at Munich from 9 January 12:00 UTC till 13 January 00:00 UTC every 12 hours. The overall features of the observations as tropospheric stability, height of the tropopause, and the evolution of the tropospheric jet stream are generally well captured by the mesoscale model results. Shutts et al. (1988) remarked that signatures of gravity waves occur as wavelike variations of temperature and wind speed in high-vertical resolution radiosonde data. It is reassuring that the mesoscale model resolves most of the temperature fluctuations with a vertical wavelength of about 2 km directly above the tropopause (e.g. see profiles b, c and d). Generally, gravity waves with vertical wavelengths larger than about 2 km can be resolved because the vertical model resolution amounts to 470 m. However, a further increase of the number of vertical levels to 99 does not improve the agreement between model results and observations significantly (Schmid, 1998).

Deviations between model profiles and radiosonde soundings generally increase with height. The model

profiles do not take into account the horizontal drift of the balloon which amounts up to 70 ... 100 km. Therefore, the magnitude of the horizontal wind is particularly concerned as small-scale variation of V_H (mainly produced by wind shift) such as visible in profiles b, c and d of Figure 10 cannot be resolved with 470 m vertical grid spacing. In this way, differences between model and radiosonde profiles become larger. Moreover, wavelike structures with greater vertical wavelength are apparent there, as well.

Stronger quantitative discrepancies are observed for the soundings that are launched at Innsbruck just once a day at 00:00 UTC (Figure 11). For these soundings only the high resolution temperature data were available, the wind profiles are plotted at the markant and standard pressure levels. Innsbruck is situated in the Inn valley at an altitude of about 580 m. The depth of the Inn valley is not completely resolved by the model orography. In the mesoscale model, Innsbruck is located at about 800 m. Therefore, the soundings start at lower heights compared to the model profiles.

The modelled temperature profiles at Innsbruck agree with the observations quite reasonable. Unfortunately, the balloon of the 11 January ascent stopped the record already at 200 hPa and therefore this sounding gives no information about the expected wave structure above the tropopause during the active mountain wave period. It may well be that the balloon burst due to strong CAT. Among other things, this assumption is confirmed by the observed low wind speed at this level. It may also be that the sonde unit automatically interrupted the record due to increase of pressure because the balloon descended for a while. Altogether, it is likely that the balloon was trapped in a region of breaking gravity waves.

The model profiles of V_H show a strong tropospheric jet (see also Figure 5b) which agrees qualitatively with the measurements. The over-estimation of the magnitude of the horizontal wind speed at lower levels is an artifact that results from insufficient model resolution of the orography. In reality, the Inn valley will excite gravity waves with horizontal wavelength of the order of 20 km. These waves are thought to be responsible for the local deceleration of the flow.

4.2 Aircraft Report Data

Two different data sources of CAT reports from aircraft are used in this study. Direct pilot reports (PIREPs) are the classical data source of turbulence encounters along air traffic routes. Usually, these reports are neither archived by airlines nor by national weather services for longer times. Fortunately, Austro Control, the aviation weather service of Austria stored PIREPs above the eastern Alpine region for the years 1995 and 1996. Most of the reports come from medium and large airplanes as A 310, B 737 and DC 10 crossing Austria and Germany; reports from Italy, Switzerland and France are not available.

The other source is the archive of automatic reports from aircraft equipped with Aircraft to Satellite Data Relay (ASDAR) systems held by the UK Meteorological Office. Up to now, these systems are exclusively carried by widebodied jets. Reports on meteorological conditions are sent every 7 minutes during the cruisephase[2] (Halsey et al., 1997). These reports also include turbulence encounters which are indicated by 0 to 3, i.e. none, light, moderate and severe turbulence (Turner, 1997). The advantages of ASDAR system reports are their regularity and objectivity, e.g. the CAT index measures the vertical acceleration of the airplane in units of gravitational acceleration g. In contrast, PIREPs depend very much of the individual feeling of pilots in the respective small, medium or heavy aircraft.

A composite of all available aircraft reports during the foehn period is plotted in Figure 12. One can clearly detect the main air traffic route on the northeastern edge of the Alpine mountain range. There, most of the turbulence encounters are reported at different flight levels but mainly on levels close to FL 330, i.e. at approximately 11 km. The absence of PIREPs over the Western Alps reflects the limited conclusive power of such a figure due to incomplete data sets. The spatial coverage of ASDAR system reports is very sparse because just 1% of all aircraft crossing the Alps per day carries such a system. Moreover, these airplanes are mostly heavy weight and turbulence events which may be hazardous to smaller aircraft are certainly undetected.

Figure 13 shows PIREPs and simulated regions of turbulence above the eastern Alps on two successive days. The respective model times are chosen in such a way that the CAT reports are close to these dates. The simulated regions where the Richardson number is less than a quarter coincide very well with the location of CAT reports. Additionally, the temporal extension of the breaking region towards west is reasonably well represented by the mesoscale model.

[2] The cruisephase is defined as period when no changes in height of more than ten feet occur during a three second period

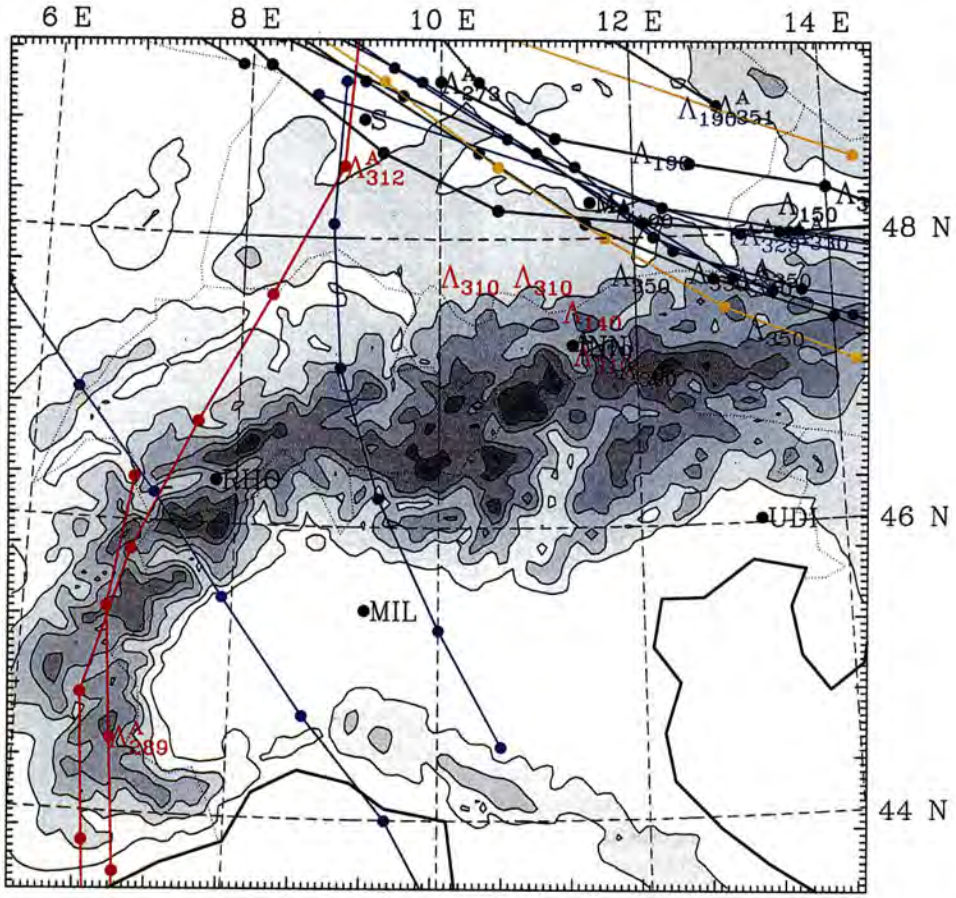

Figure 12: Pilot reports (PIREP's) of turbulence above the Alps during the foehn period from 8 January to 13 January 1996. Turbulence encounters are indicated by Λ_{FL} where the corresponding flight level FL gives the altitude in the standard atmosphere above the 1013 hPa surface in feet divided by 100. ASDAR system reports of individual aircraft are joined by lines. Turbulence is marked by Λ^{A}_{FL}) and the colour coding indicates the date (8 January: light blue; 9 January: black; 10 January: blue; 11 January: green; 12 January: red; 13 January: yellow).

5 Discussion and Conclusions

In this study, a high-resolution mesoscale model with horizontal mesh size of 6 km is used to simulate the upper-level wave breaking above the Alps. The mesoscale simulations reproduce the crucial features of the long-lasting south foehn event of January 1996. Vertical profiles of V_H and T, the location and duration of turbulence regions confirm available observations by radiosondes, PIREPs and ASDAR system reports. Therefore, mesoscale models even with simplified model physics (no moisture, no radiation) but with high horizontal and vertical resolution are considered as essential component for a realistic simulation of breaking regions over complex topography as that of the Alps. In this way, the results of this case study can be understood as a first step to establish confidence in mesoscale model simulations to forecast breaking gravity waves and meteorological conditions where CAT is produced.

Relating the occurrence of breaking gravity waves to synoptic-scale conditions during the south foehn event, the present study permits the following conclusions:

- Strong low-level winds perpendicular to the main Alpine ridge and a substantially thick layer that passes over the Alps (i.e. $\mathcal{F} > 1$ for a $z < h_0$),
- minimum directional wind shear with height, and
- a southerly jet stream of sufficient strength

are essential for the generation of gravity waves and its vertical propagation up to the upper troposphere/lower stratosphere. Amplifying of wave amplitude with height as well as the large vertical shear lead to regions of small Richardson numbers which become negative in overturning waves. These regions above and in the lee of the Alps are likely locations for CAT encounters of crossing aircraft. The downwind extension of these CAT regions of about

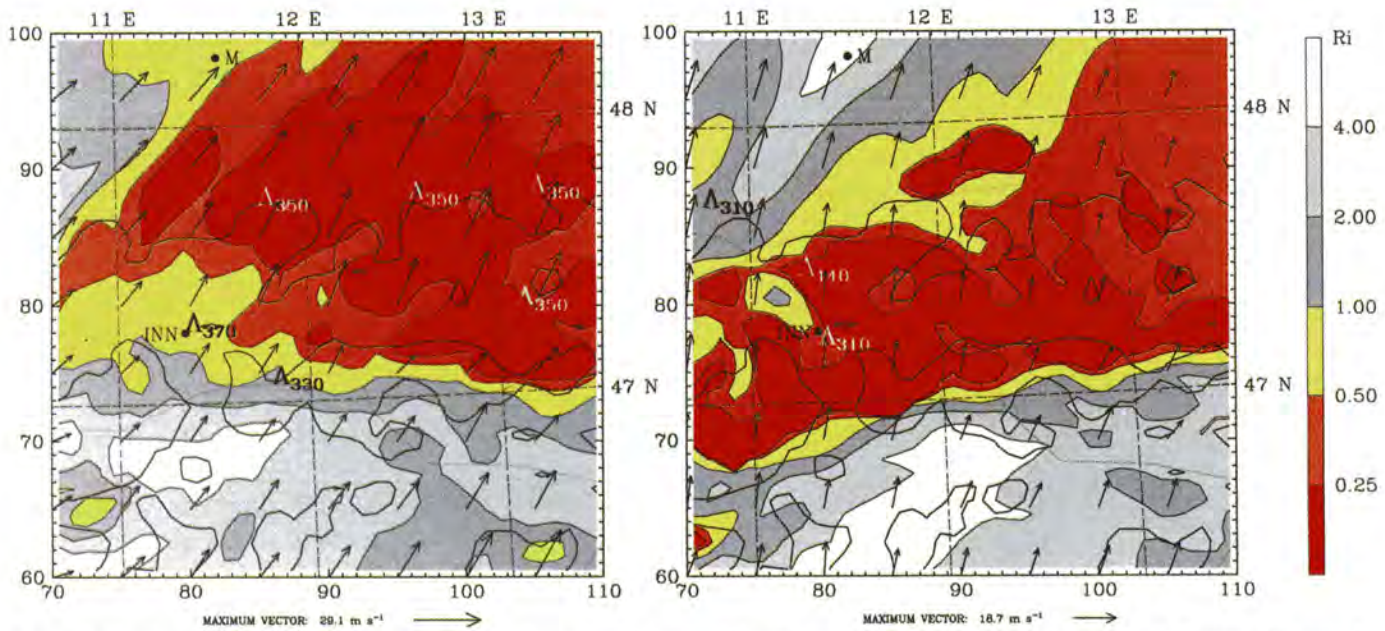

Figure 13: Composite of minimum Richardson number (cf. Figure 6b) and turbulence encounters (PIREPs, cf. Figure 12) over the eastern Alps. Left (right) simulated Richardson numbers at 11 January 18:00 UTC (12 January 12:00 UTC); 11 January: PIREPs for FL 350 are valid at 20:00 UTC; 12 January: PIREPs for FL 310 are valid at 14:30 UTC; the others reports are at earlier dates.

100 ... 150 km is caused by the continuously large vertical shear around the jet stream.

The quality of the CAT prediction based on the Richardson number depends *inter alia* on the vertical resolution of the numerical model. The coarser the resolution, the more uncertain the prediction of small Richardson numbers. Therefore, Lee et al. (1979) proposed an empirically developed relationship between the bulk Richardson number Ri_B as used in large-scale models, and the probability of turbulence occurrence. This relates values of Ri_B smaller than 1 to a turbulence probability of over 90% . In this sense, regions of $Ri < 1$ indicate the possibility of producing CAT even in mesoscale simulations.

Direct observations of breaking internal gravity waves are rare. During the MAP field phase in autumn 1999 an international effort will be made to observe upper-level wave breaking by remote sensing and *in-situ* methods. With respect to these campaigns and from the modellers point of view, a better availability and higher spatial coverage of meteorological data of the free atmosphere would be desirable. These include high-vertical resolution radiosonde soundings launched at least every six hours, PIREPs of all type of aircraft for the Alpine region. Moreover, standard meteorological observations of commercial aircraft are very useful for completing the picture of the complex thermodynamic atmospheric state above the Alps. Lidar data and second-moment data from wind profilers are valuable to quantify the turbulence intensity. These data could enable detailed comparisons with mesoscale model results.

Additionally, high-resolution model intercomparison studies will be performed before the field phase as envisaged by the MAP-Science plan (Bougeault et al., 1998). Eventually, high-resolution models can be used for real-time forecasts to guide measurements during the ongoing MAP field phase as it was done for Arctic campaigns by Dörnbrack et al. (1998).

Another possibility to improve flight safety for airline passengers is the compilation of a model-based climatology of CAT above the Alps. The statistical-dynamical downscaling technique represents a suitable method that is based on a multi-year set of large-scale analyses that represent the current climate (e.g. ECMWF re-analyses data) and non-hydrostatic mesoscale simulations (Fuentes and Heimann, 1996; Heimann, 1997). Such a climatology can assist aviation weather forecasters in effective air route planning and helps to prevent turbulence injuries and accidents.

Considerable progress in forecasting wave breaking events over orography can be expected if future work, proceeding along the lines of this study, accumulates further evidence that the numerical prediction of time and location of breaking gravity waves is feasible.

Acknowledgements

We thank Judith Turner (UK MetOffice, Bracknell) for kindly providing the ASDAR system reports. Dr. Abel (Austro Control, Vienna) opened his archive and recovers the treasures of PIREPs for this study. Herbert Pümpel (Austro Control, Innsbruck) and Mr. Limberger (DWD, Oberschleißheim) sent us the high-vertical resolution radiosonde data of Innsbruck and Munich. We express our thanks to Martin Leutbecher, Dietrich Heimann, Hans Volkert, Branko Grisogono and James Doyle for their critical comments on an early version of the manuscript.

References

Baines P.G., 1995: Topographic effects in stratified flows. Cambridge University Press, 482pp.

Bougeault P., Binder P., and Kuettner J., 1998: MAP Science Plan. Zürich, (also: `http://www.map.ethz.ch/splan/spindex.htm`).

Binder P. and Schär C., 1996: MAP Design Proposal, Second Edition. Zürich, (also: `http://www.map.ethz.ch/proposal.htm`).

Booker J.R. and Bretherton F.P., 1967: The critical layer for internal gravity waves in a shear flow. J. Fluid Mech. **27**, 513–539.

Dörnbrack A., 1998: Turbulent mixing by breaking gravity waves. J. Fluid Mech. **375**, 113–144.

Dörnbrack A., Leutbecher M., Volkert H., and Wirth M., 1998: Mesoscale forecasts of stratospheric mountain waves. Meteorol. Appl. **5**, 117–126.

Dutton J.A. and Panofsky H.A., 1970: Clear air turbulence: A mystery may be unfolding. Science **167**, 937–944.

Fuentes U. and Heimann D., 1996: Verification of statistical-dynamical downscaling in the Alpine region. Clim. Res. **7**, 151–168.

Grell G.A., Dudhia J., and Stauffer D.R., 1994: A description of the fifth-generation Penn State/NCAR mesoscale model (MM5). Techn. Note 398, National Center for Atmospheric Research, Boulder, CO, 121 pp.

Halsey N.G.J., McHaffie A., Forrester D.A., and Lunnon, R.W., 1997: Investigation of current clear-air turbulence (CAT) algorithms, using the UK Met Office aviation group's archives of automated aircraft reports. Proc. Seventh AMS-Conference on Aviation, Range, and Aerospace Meteorology, Long Beach, CA, 197–201.

Heimann D., 1997: Mesoscale surface wind characteristics and potential gravity wave formation during cross alpine airflow. Meteorol. Atmos. Phys. **62**, 49–70.

Hoinka K.-P., 1990: Untersuchung der alpinen Gebirgsüberströmung bei Südföhn. DLR-FB 90-30, 186pp.

Keller J.L., 1990: Clear air turbulence as a response to meso- and synoptic-scale dynamic processes. Mon. Wea. Rev. **118**, 2228–2242.

Knox J.A., 1997: Possible mechanisms of clear-air turbulence in strongly anticyclonic flows. Mon. Wea. Rev. **125**, 1251–1259.

Lee D.R., Stull R.B. and Irvine W.S., 1979: Clear air turbulence forecasting techniques. AFGWC/TN-79/001. Air Force Global Weather Central, Offutt AFB, NE 68113, 73pp.

Leutbecher M., 1998: Die Ausbreitung orographisch angeregter Schwerewellen in die Stratosphäre – Lineare Theorie, idealisierte und realitätsnahe numerische Simulation. PhD thesis Ludwig-Maximilians-Universität München. Rep. FB–98-17 available from Deutsches Zentrum für Luft- und Raumfahrt, D-51170 Köln, Germany.

Lilly D.K., 1978: A severe downslope windstorm and aircraft turbulence event induced by a mountain wave. J. Atmos. Sci. **35**, 59–77.

Pierrehumbert R.T. and Wyman B., 1985: Upstream effects of mesoscale mountains. J. Atmos. Sci. **42**, 977–1003.

Ralph F.M., Neiman P.J., and Levinson D., 1997: Lidar observations of a breaking mountain wave associated with extreme turbulence. Geophys. Res. Let. **24**, 663–666.

Schmid H., 1998: Clear-Air Turbulence bei Südföhn – Eine Fallstudie. Dipl. Thesis, Meteor. Institut der Ludwig-Maximilians-Universität München.

Sheppard R.S., 1956: Airflow over mountains. Q. J. R. Meteorol. Soc. **82**, 528–529.

Shutts G., 1995: Gravity-wave drag parametrization over complex terrain: The effect of critical-level absorption in directional wind-shear. Q. J. R. Meteorol. Soc. **121**, 1005–1021.

Shutts G.J., Kitchen M., and Hoare P.H., 1988: A large amplitude gravity wave in the lower stratosphere detected by radiosonde. Q. J. R. Meteorol. Soc. **114**, 579–594.

Smith R.B., 1977: The steepening of hydrostatic mountain waves. J. Atmos. Sci. **34**, 1634–1654.

Smith R.B., 1979: The influence of mountains on the atmosphere. Adv. in Geophysics **21**, 87–230.

Snyder W.H., Thomson R.S., Lawson R.E., Castro I.P., Lee J-T.; Hunt J.C.R., and Ogawa Y., 1985: The structure of strongly stratified flow over hills: dividing streamline concept. J. Fluid Mech. **152**, 249–288.

Turner J.A., 1997: The use of gravity wave drag parameters to predict mountain wave turbulence for civil aviation. Forecasting Res. Div. – Techn. Report No. 221, Meteorological Office, London Road, Bracknell, Berkshire, RG12 2SZ, UK.

Wurtele M.G., Sharman R.D. and Datta A., 1996: Atmospheric Leewaves. Ann. Rev. Fluid Mech. **28** 429–476.